PHYSICAL REVIEW C VOLUME 25, NUMBER 3 MARCH 1982

Dynamics of nuclear fluid. VIII. Time-dependent Hartree-Fock approximation from a classical point of view

Cheuk-Yin Wong
Oak Ridge National Laboratory, Oak Ridge, Tennessee 37830
(Received 3 September 1981)

In order to facilitate the comparison of the time-dependent Hartree-Fock approximation with other classical theories and to help guide our intuition in understanding the underlying physics, we study the time-dependent Hartree-Fock approximation from a classical viewpoint. We show that the time-dependent Hartree-Fock approximation is approximately equivalent to a purely classical pseudoparticle simulation. In this simulation, a collection of pseudoparticles is introduced to discretize the phase space of spatial and momentum coordinates. The dynamics is completely determined by following the pseudoparticle trajectories which are the same as the trajectories of real particles moving in the self-consistent field. As an application of the concept of the pseudoparticle simulation, we study the origin of the nonfusion events in nearly-head-on heavy-ion collisions as obtained in the time-dependent Hartree-Fock approximation. It is argued that for these nearly-head-on collisions, the emergence of the most energetic pseudonucleons of one nucleus outside the far surface of the other nucleus initiates a coherent flow-through motion because of self-consistency and leads to the breakup of the composite system. Based on this picture, we obtain quantitative estimates of the threshold energies and the low-l fusion window which agree quite well with the time-dependent Hartree-Fock results.

[NUCLEAR REACTIONS Time-dependent Hartree-Fock approximation. Vlasov equation. Pseudoparticle simulation. Low-l fusion window in heavy-ion collisions.]

I. INTRODUCTION

This is one of a series of articles dealing with the dynamics of nuclear fluid. Other studies concern themselves with the equations governing the dynamics starting with time-dependent Hartree-Fock approximations (TDHF),[1] the generalization to include spin and isospin degrees of freedom,[2] the kinetic theory of quantum fluids,[3] and the extension of the time-dependent Hartree-Fock approximation to include particle collisions.[4] We present here a study of the time-dependent Hartree-Fock approximation from a classical viewpoint and shall show the approximate equivalence of the TDHF approximation and a classical pseudoparticle simulation in which the dynamics is described in terms of pseudoparticles following classical collisionless trajectories in their self-consistent potential.[5]

Recent renewed interest in the time-dependent Hartree-Fock approximation (TDHF) for the microscopic description of the dynamics of nuclear systems was pioneered by Bonche, Koonin, and Negele.[6] Since then, many TDHF calculations were carried out[7–11] and many different theoretical investigations were initiated.[12–20,1–5] In the TDHF approximation, the fermions are assumed to interact only through the mean field and the collisions between particles due to residual interactions are negelected. The knowledge of the initial wave functions of the fermions allows one to trace the subsequent behavior of the nuclear system. Numerical solutions[6–11] of the TDHF equations provide interesting insight into the dynamics of the interacting fermion systems.

It is of interest to examine the time-dependent Hartree-Fock approximation from a classical viewpoint. The approximate transcription of the time-dependent Hartree-Fock approximation into a purely classical model helps guide our intuition and provides a deeper understanding of the underlying physics involved. In fact, we shall later see that such a classical picture helps us understand the origin of the low-l nonfusion events in the TDHF calculations of heavy-ion collisions.

Recently, a simple classical model[21] was put forth for the discussion of low-energy fermion dynamics. The theory of one-body dissipation makes simple assumptions concerning the trajectories of nucleons and the dissipation of collective energies. Much progress has been made in justifying the theory from the linear response theory.[22] A numerical comparison with the TDHF results has also been made.[11] Comparison of the similarities and differences between the TDHF approximation and the theory of one-body dissipation can be facilitated with a classically-equivalent description of the TDHF approximation.

Classical many-body theory has also been used recently to investigate the collision of two nuclei at high energies.[23–31] The theoretical justification of such an approach usually starts from a classical description of the dynamics from the beginning. Comparison of the classical transcription of the TDHF approximation with these models will be of use in revealing ways in which these models can be modified to include the effects of the mean field.

The approximate equivalence of the TDHF approximation and a classical pseudoparticle simulation can be made by going to the Wigner space. It has long been known that in the Wigner space, if one interprets the Wigner function as a classical distribution function and takes the limit of $\hbar \to 0$, then one obtains from quantum mechanical equations of motion purely classical equations of motion.[32–35,3] By following a similar procedure for the TDHF approximation, we are guaranteed to obtain classical equations of motion for the dynamics, which in this case is the Vlasov equation involving the mean-field potential. The next crucial step is to decompose the phase space in terms of a collection of pseudoparticles having definite phase space coordinates. The equations of motion of these pseudoparticles are then the classical Newtonian equations of motion involving the self-consistent potential. The approximate equivalence of the TDHF approximation and the pseudoparticle simulation is thus exhibited.

Although the equation of motion can be purely classical, there are quantum effects which exert a great influence on the dynamics. With the classical equations of motion, the dynamics is completely determined by the initial conditions. It is in the initial conditions where important quantum effects can be introduced. In the TDHF approximation, the Pauli exclusion principle for the occupation of single-particle states leads to an equilibrium phase space distribution nearly uniform in a phase space region. In the classical pseudoparticle simulation, a collection of pseudoparticles with a similar phase space distribution will lead to an equilibrium. However, because of the nonlinear nature of the dynamics, other types of equilibrium distribution are also possible. The adherence to the Pauli principle requires that we choose the equilibrium distribution as the one close to that obtained from the Hartree-Fock calculations. Once such an equilibrium distribution is chosen, the incompressibility of the phase space fluid guarantees that the Pauli principle will not be later violated in the subsequent stages of the dynamical motion.

Although particle simulation models have been used extensively in molecular dynamics,[36] nuclear collisions,[23–31] and plasma physics,[37] the ones which come closest to the TDHF approximation are those in plasma physics where the mean-free paths of the constituent particles are so large that the dynamics can be well approximated to be collisionless. Much progress in using particle simulation models to study plasma dynamics has been made recently; three-dimensional codes have been developed to trace the trajectories of about one-half million particles in order to study the detailed dynamics of electrons and ions in controlled fusion devices.[37] Similar techniques may perhaps be applied to the dynamics of nucleons in heavy-ion collisions, although the need to trace the trajectory of a large number of the pseudoparticles may make the calculation infeasible.

The pseudoparticle simulation of nuclear dynamics can be readily utilized to understand some special features of the TDHF results. Recent TDHF calculations[7–13] indicate that for nearly-head-on collisions above the Coulomb barrier, there is a threshold energy above which no fusion of the composite system takes place. By following the trajectories of the nucleons, we argue that for these nearly-head-on collisions, the emergence of the most energetic pseudonucleons outside of the far surface of the other nucleus initiates a flow-through motion because of the self-consistent effects and leads to the breakup of the composite system. Based on such a simple picture, estimates of the threshold energies and l window are obtained and found to agree well with the TDHF calculations, indicating the approximate validity of such a picture. The condition for the onset of fast particle emission in a fusion reaction is also determined.

This paper is organized as follows: In Sec. II, we start with the TDHF approximation and show how it can lead to the pseudoparticle simulation. The important approximations and the difference be-

tween pseudoparticles and real particles are spelled out. In Sec. III, a numerical example of pseudoparticle simulation is carried out and compared with the TDHF approximation. In Sec. IV, we discuss the low-l fusion window and fast particle emission in TDHF calculations. We suggest that a flow-through motion, due to the emergence of the most energetic pseudonucleons at the far side of the other nucleus, may be the origin of the breakup of the composite system. Quantitative estimates based on this picture give good agreement with the TDHF results. Section V summarizes and concludes the present discussion.

II. PSEUDOPARTICLE SIMULATION AS A CLASSICAL APPROXIMATION OF TDHF

The equation of motion for a single-particle state in the TDHF approximation is given by

$$i\hbar\frac{\partial}{\partial t}\psi_\lambda(\vec{r},t)=\left[-\frac{\hbar^2}{2m}\nabla^2+\mathscr{V}(\rho(\vec{r},t))\right]\psi_\lambda(\vec{r},t)\ . \tag{2.1}$$

Here, m is the mass of a nucleon, and for simplicity, we have averaged out the spin and isospin degrees of freedom. The mean-field potential $\mathscr{V}(\rho(\vec{r},t))$ is

$$\mathscr{V}(\rho(\vec{r},t))=\int d^3r_2[v_s(\vec{r}-\vec{r}_2)+v_l(\vec{r}-\vec{r}_2)]\rho(\vec{r}_2)\ , \tag{2.2}$$

where the short-range effective potential v_s is density dependent and given, for example, by[6]

$$v_s(\vec{r}-\vec{r}_2)=[\tfrac{3}{4}t_0+\tfrac{3}{16}t_3\rho(\vec{r})]\delta(\vec{r}-\vec{r}_2)\ , \tag{2.3}$$

and v_l is the long-range Coulomb and Yukawa interaction

$$v_l(\vec{r}-\vec{r}_2)=\beta\frac{e^{-\alpha|\vec{r}-\vec{r}_2|}}{|\vec{r}-\vec{r}_2|}+\frac{e^2}{4|\vec{r}-\vec{r}_2|}\ . \tag{2.4}$$

The density is given by

$$\rho(\vec{r})=\sum_\lambda^{\text{occ}}|\psi_\lambda(\vec{r})|^2\ . \tag{2.5}$$

The set of parameters t_0, t_3, β, and α can be found, for example, in the work of Bonche *et al.*[6]

In order to study the TDHF approximation from a classical viewpoint, we go to the Wigner space $(\vec{r},\vec{p})$ where the correspondence between classical mechanics and quantum mechanics can be readily made. The procedure to accomplish this is well known.[32–35,3] We shall briefly review the pertinent results and introduce the Lagrangian picture of the phase space fluid elements as our main tool to discuss the dynamics.

The (reduced one-body) Wigner function for a system of independent particles is given by

$$f(\vec{r}\,\vec{p},t)=\int d\vec{s}\,e^{i\vec{p}\cdot\vec{s}/\hbar}\sum_\lambda^{\text{occ}}\psi_\lambda(\vec{r}-\vec{s}/2,t)\times\psi_\lambda^*(\vec{r}+\vec{s}/2,t)\ , \tag{2.6}$$

where the summation over λ extends over the occupied states. The equation of motion for the Wigner function in the TDHF approximation is[32–35,3]

$$\frac{\partial f}{\partial t}(\vec{r}\,\vec{p},t)+(\vec{p}/m)\cdot\vec{\nabla}_r f(\vec{r}\,\vec{p},t)-\frac{2}{\hbar}\sin\left[\frac{\hbar}{2}\vec{\nabla}_r^v\cdot\vec{\nabla}_p^f\right]\mathscr{V}(\rho(\vec{r},t))f(\vec{r}\,\vec{p},t)=0\ , \tag{2.7}$$

where the superscripts v and f refer to the functions on which the gradient operators apply.

Given the Wigner function $f(\vec{r}_0\vec{p}_0,t_0)$ at time t_0, we wish to develop a Lagrangian picture for the Wigner function $f(\vec{r}\,\vec{p},t)$ at a slightly later time $t=t_0+\delta t$. We write the solution in the form

$$f(\vec{r}\,\vec{p},t)=\int d\vec{r}_0 d\vec{p}_0\int\frac{d\vec{s}}{(2\pi\hbar)^3}\exp\{i\vec{s}\cdot[\vec{p}-\vec{P}(\vec{r}_0\vec{p}_0\vec{s},t)]/\hbar\}\delta[\vec{r}-\vec{R}(\vec{r}_0\vec{p}_0,t)]f(\vec{r}_0\vec{p}_0,t_0)\ . \tag{2.8}$$

The equations of motion for $\vec{P}$ and $\vec{R}$ are then

$$\frac{\partial\vec{R}}{\partial t}=\frac{\vec{p}}{m}\ , \tag{2.9}$$

$$\vec{s}\cdot\frac{\partial\vec{P}}{\partial t}=\mathscr{V}\left[\vec{R}-\frac{\vec{s}}{2}\right]-\mathscr{V}\left[\vec{R}+\frac{\vec{s}}{2}\right]\ . \tag{2.10}$$

For small increments of time, we have

$$f(\vec{r}\vec{p},t)=\int d\vec{p}_0 \int \frac{d\vec{s}}{(2\pi\hbar)^3}\exp i\left\{\left\{\vec{s}\cdot(\vec{p}-\vec{p}_0)+\left[\mathscr{V}\left[\vec{R}+\frac{\vec{s}}{2}\right]-\mathscr{V}\left[\vec{R}-\frac{\vec{s}}{2}\right]\right]\delta t\right\}/\hbar\right\} f(\vec{r}-\vec{p}\delta t,\vec{p}_0,t_0)\ , \tag{2.11}$$

where the right hand side involves only known functions and can be integrated, in principle, at the least.

When terms up to the fifth-order derivatives of are neglected, we have

$$f(\vec{r}\vec{p},t)\cong \int d\vec{r}_0 d\vec{p}_0 \delta[\vec{r}-(\vec{r}_0+\vec{p}\delta t)]\Delta\{\vec{p}-[\vec{p}_0+\nabla\mathscr{V}(\vec{r})]\}f(\vec{r}_0\vec{p}_0,t) \tag{2.12}$$

where the packet in momentum Δ is given by

$$\Delta(\vec{x})=\int \frac{d\vec{s}}{(2\pi\hbar)^3}\exp\left\{i\left[\vec{s}\cdot\vec{x}+\frac{1}{6}\sum_{ijk}^{3}s_i s_j s_k \nabla_i\nabla_j\nabla_k\mathscr{V}\right]/\hbar\right\}. \tag{2.13}$$

In the special case when $\mathscr{V}$ depends locally only on one of the coordinates r_i and not on $\vec{r}_\perp$, the packet Δ becomes a product of a two-dimensional delta function and an Airy function[38]

$$\Delta(\vec{x})=\delta(\vec{x}_\perp)\frac{1}{2\pi(3a)^{1/3}}Ai\left[\frac{x_i}{(3a)^{1/3}\hbar}\right] \tag{2.14}$$

and

$$a=\frac{1}{24\hbar}\,|\,\nabla_i{}^3\mathscr{V}(\vec{r})\,|\,\delta t\ . \tag{2.15}$$

The results of Eq. (2.15) are not of practical use as the Δ packet is not simple in the general case. The oscillatory nature of Δ also leads to negative values of $f(\vec{r}\vec{p},t)$ in the tail region of the Wigner function.

A direct numerical solution of the time dependence of the Wigner function can be obtained by first solving the TDHF equation (2.1) and then constructing the Wigner function afterwards.[39] This procedure appears simpler than solving Eq. (2.7) directly. The study of the time dependence of $f(\vec{r}\vec{p},t)$ with Eq. (2.7) and its approximation serves a different purpose. Our objective, however, is to have an understanding of the underlying physics involved in a TDHF approximation. As classical physics is very useful in guiding our intuition, we seek a classical approximation of Eq. (2.7).

As is well known, the Wigner function is analogous with, but not identical to, the distribution function in classical mechanics. In order to provide greater insight and to guide our intuition in the dynamics of the fermion system, we shall go to the classical limit and adopt the interpretation of the Wigner function as the classical distribution function.[32–35,3] This can be achieved by expanding $\mathscr{V}$ only up to the first spatial derivative in Eqs. (2.7) and (2.11). Equation (2.7) then becomes the well-known Vlasov equation and the Lagrangian picture of the Wigner function as given by Eq. (2.11) becomes

$$f(\vec{r}\vec{p},t)=\int d\vec{r}_0 d\vec{p}_0 \delta[\vec{r}-\vec{R}(\vec{r}_0\vec{p}_0 t)]\times\delta[\vec{p}-\vec{P}(\vec{r}_0\vec{p}_0 t)]f(\vec{r}_0\vec{p}_0,t_0)\ , \tag{2.16}$$

where $\vec{R}$ and $\vec{P}$ satisfy the classical equation of motion

$$\frac{d\vec{R}}{dt}=\frac{\vec{P}}{m} \tag{2.17}$$

and

$$\frac{d\vec{P}}{dt}=-\nabla_R\mathscr{V}(\rho) \tag{2.18}$$

with

$$\rho(\vec{R})=\int \frac{d^3\vec{P}}{(2\pi\hbar)^3}f(\vec{R}\vec{P},t)\ . \tag{2.19}$$

The above results allow us to formulate a pseudoparticle simulation as an approximation of the TDHF approximation. Our first task is to discretize the Wigner space into cells (pseudoparticles). The total number N_p of cells (pseudoparticles) depends on the fineness of discretization and need not relate directly to the actual number of real constituent particles. Each cell element λ is characterized by initial coordinates $\vec{r}_i$ and $\vec{p}_i$ at time t_0 with a weight of $f(\vec{r}_i\vec{p}_i,t_0)$. Our next task is to obtain solutions of the trajectory functions $\vec{R}$ and $\vec{P}$ by solving the classical equation of motion Eqs. (2.17) and (2.18). The density function ρ can then be

evaluated with Eq. (2.19) from the distribution function to generate the self-consistent potential at the new time coordinate. In this step-wise manner, the distribution function can be obtained as a function of time in terms of trajectories of pseudoparticles.

It is important to realize that the time development of the point $(\vec{R},\vec{P})$ is exactly identical to that of a single particle of mass m traversing in the potential $\mathscr{V}$. Because of such identity, it is convenient to refer to these cells in the Wigner space as pseudoparticles. However, these pseudoparticles are introduced in the discretization of the Wigner space. The density and sizes of pseudoparticles depends on the fineness of discretization. In contrast, the density of real particles are obtained by integrating the distribution function over the momentum coordinates. These two densities are clearly different; so are the numbers of real and pseudoparticles.

III. A NUMERICAL EXAMPLE

In order to assess the pseudoparticle simulation as a useful concept, we wish to carry out some numerical calculations and compare them with the TDHF calculations. They allow us to bring out the peculiar characteristics of the pseudoparticle simulation which can help guide our intuition in nuclear dynamics.

The numerical calculation can be readily made for the collision of two nuclear slabs. We use the same force and parameters as those of Bonche, Koonin, and Negele.[6] We examine the collision of two slabs each of which has a "total mass" of $\mathscr{A}_1=\mathscr{A}_2=1.4$ fm^{-2}. The initial trial distribution function $\bar{f}(z,k_x,k_y,k_z)$ is taken to be a Fermi distribution with a width of $\Delta k^2=0.01$ fm^{-2}

$$\bar{f}(z,k_x,k_y,k_z)=\frac{1}{1+\exp\{[(k_x^2+k_y^2+k_z^2)+2m(\mathscr{V}(\rho)-\epsilon_f)/\hbar^2]/\Delta k^2\}} . \tag{3.1}$$

Following Bonche *et al.*, we shall freeze the momentum in the transverse direction. It is only necessary to consider the distribution function $f(z,k_z)$ after integrating $\bar{f}$ over k_x and k_y

$$f(z,k_z)=\frac{(\Delta k^2)}{4\pi}\ln(1+\exp\{[2m(\mathscr{V}(\rho)-\epsilon_f)/\hbar^2-k_z^2]/\Delta k^2\}) , \tag{3.2}$$

which is normalized according to

$$\int (dk_z/2\pi)f(z,k_z)=\rho(z) \tag{3.3}$$

and

$$\int dz(dk_z/2\pi)f(z,k_z)=\mathscr{A}=\mathscr{A}_1+\mathscr{A}_2 . \tag{3.4}$$

Using Eq. (3.1) and an assumed $\rho(z)$ and ϵ_f, we decompose the distribution into N_p pseudoparticles each of which occupies a volume of $\mathscr{A}/N_p$ in the (z,k_z) space. After the decomposition, the pseudoparticle number and coordinates, $\mathscr{V}(\rho)$ and ϵ_f, are readjusted by iteration until a self-consistent set of pseudoparticles characterized by coordinates (z_i,k_{zi}) is obtained as the starting point of the dynamical calculation. Each pseudonucleon is then given an additional velocity to bring the slabs towards each other. At each time step, the density is evaluated by giving a Gaussian distribution in space to each pseudoparticle so that the density is

$$\rho(z)=\frac{\mathscr{A}}{N_p}\sum_i^{N_p}\frac{e^{-(z-z_1)^2/2\sigma^2}}{\sqrt{2\pi}\sigma} , \tag{3.5}$$

where σ is taken to be the size of the mesh. From the density, the potential is obtained as in Eq. (2.2). The forces acting on the pseudoparticles are calculated and the new pseudoparticle coordinates (z_i,k_{zi}) are determined by solving Eqs. (2.17) and (2.18). The densities are then obtained again to start a new time cycle of the dynamics.

In our calculations, we use about $N_p=7200$ pseudoparticles to describe the dynamics. We employ the fast Fourier transform method to calculate the potentials. In order to compare our results with the time-dependent Hartree-Fock calculations, the high-frequency Fourier components need to be truncated[10] as they correspond to the inclusion of very high-lying single-particle basis states or alternatively the inclusion of higher-order spatial finite differences. Accordingly, we keep in the potential only those Fourier components corresponding to an energy less than twice the Fermi energy.[10] While this may give a good comparison with the TDHF results, the solutions of the Vlasov equation involves many more degrees of freedom and may otherwise produce very fine spatial density oscillations which

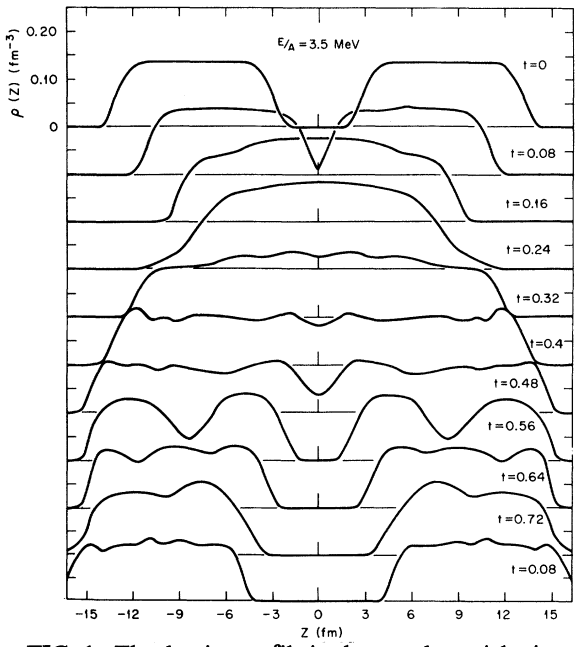

FIG. 1. The density profile in the pseudoparticle simulation for the collision of two slabs with $\mathscr{A}_1=\mathscr{A}_2=1.4$ fm^{-2} at the center-of-mass bombarding energy of $E/A=3.5$ MeV. The time scale is in units of 10^{-2} sec.

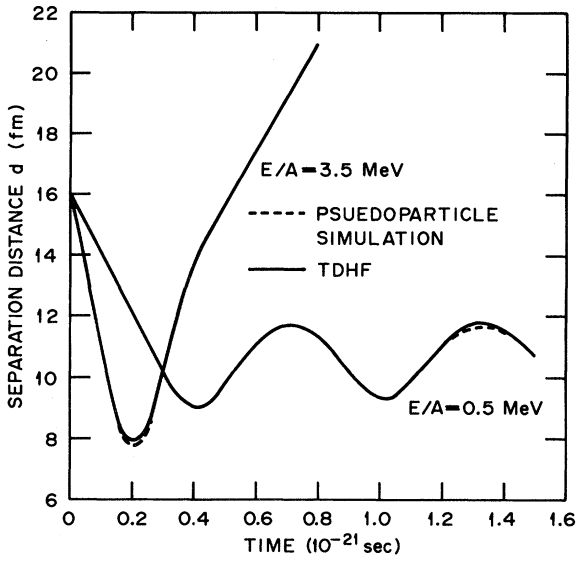

FIG. 2. The time dependence of the fragment separation coordinate d for the collision of two slabs at the center-of-mass bombarding energies of $E/A=0.5$ MeV and $E/A=3.5$ MeV. The results of the pseudoparticle simulation is given by the dashed line, while the TDHF results (from Fig. 8 of Ref. 6) are given by the solid line.

are not physical for finite nucleon systems.

We shall examine the dynamics at two different energies: $E/A=3.5$ MeV and $E/A=0.5$ MeV in the center-of-mass system. Figure 1 shows the density profile for the case of $E/A=3.5$ MeV. The slabs are initially separated at 16 fm. At $t=0.24\times10^{-21}$ sec, the system reaches its maximum density of about 0.19 nucleons/fm^3. The density drops rapidly afterwards as the system stretches outward. At about $t=0.48\times10^{-21}$ sec, a density depression begins to develop around $z=0$. The two slabs rapidly separate into two different pieces and move away from each other with a speed much less than the incident speed. Upon comparing the dynamics with those of the TDHF at the same energy, one finds that the density profile is quite similar to those in the TDHF calculations. There, density maximum is also reached at $t\simeq0.24\times19^{-21}$ sec and the slabs begin to separate with respect to each other at $t\simeq0.48\times10^{-21}$ sec.[6] In fact, we can define a separation distance d as

$$d=\int_{-\infty}^{\infty}|z|\rho(z)dz\ , \tag{3.6}$$

and plot d as a function of time in Fig. 2. One finds that $d(t)$ for the two different calculations follow each other quite closely. For the other case when $E/A=0.5$ MeV, the two slabs fuse together to form a combined system. The gross features of the density profiles in the pseudoparticle simulation are similar to those of the TDHF calculation. The separation distance d as a function of time t is also displayed in Fig. 2. One finds that for this energy of $E/A=0.5$ MeV, the dynamics from the two different calculations are very similar.

In spite of the close similarity of the results of the two different calculations, there are nevertheless small differences. For example, the compression for $E/A=3.5$ MeV at $t\simeq0.24\times10^{-21}$ sec is slightly greater for the pseudoparticle simulation than it is for the TDHF calculation (Fig. 2). The oscillations of the density are slightly more pronounced in the pseudoparticle simulation than in the TDHF calculation. The phases of the oscillations are also slightly different which may affect the locations of the "resonance-type" behavior between 1 and 2 MeV.[6]

An important peculiar characteristic of the pseudoparticle simulation is to allow one to exhibit the trajectories of some typical pseudonucleons so as to gain a clear insight into the dynamics of nuclear systems in heavy-ion dynamics. We plot in Fig. 3 the trajectories of six pseudonucleons of the left slab in the collision of $E/A=3.5$ MeV. They are initially located at the far side (relative to the other slab) in Figs. 3(a) and (d), the central region in Figs. 3(b)

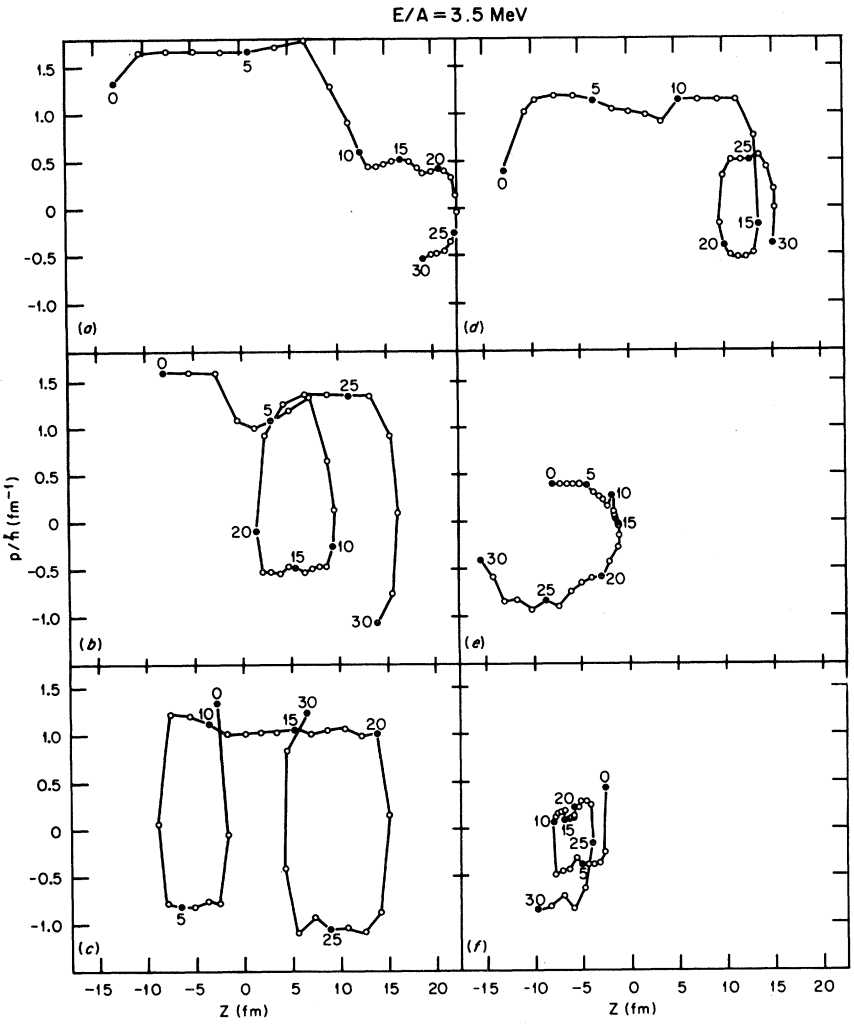

FIG. 3. The trajectories of six selected pseudonucleons for the collision of two slabs at a center-of-mass bombarding energy of $E/A = 3.5$ MeV. The trajectories are linked by straight lines. The positions at time steps 0, 5, 10, 15, . . . are given by solid points and their time step numbers are also indicated. The time step Δt is 0.0267×10^{-21} sec. Pseudonucleons in (a), (b), and (c) initially have the greatest momenta in their corresponding locations, while the pseudonucleons in (d), (e), and (f) initially have the smallest momenta. Pseudonucleons at (a) and (d) are initially located at the far side of the left slab, pseudonucleons at (b) and (e) in the central region, and pseudonucleons at (c) and (f) at the inner edge.

and (e) and at the inner edge in Figs. 3(c) and (f). The pseudonucleons in Figs. 3(a), (b), and (c) initially have the greatest momenta at their corresponding locations, while the pseudonucleons in Figs. 3(d), (e), and (f) initially have the smallest momenta. In Fig. 3, the time sequences are labeled by the time-step numbers, each step being 0.0267×10^{-21} sec. At about the fifth time step, the boundary between the two slabs begins to disappear, and at about the nineteenth step, the two slabs separate.

We shall describe in some detail the trajectories of the pseudonucleons. The pseudonucleon in Fig. 3(a) starts at the far side of the left slab and has the greatest momentum among pseudonucleons at that point. At the fifth time step, it reaches the inner boundary. As the boundary has already disappeared, the pseudonucleon goes from the left slab into the right slab instead of returning to the right slab to replenish pseudonucleons in the left slab. It arrives at the wall of the far side of the right slab at the seventh step and begins to slow down. However, the momentum of this pseudonucleon (the leading particle) is so large that it goes over the potential well at the eleventh step and begins to emerge outside the far side of the right slab. As it emerges, it lowers the potential at the far side and allows

more and more pseudonucleons to come out. It reaches the new wall formed by the spilled pseudonucleons at the twenty-second step and bounces back from the wall.

The pseudoparticle in Fig. 3(b) starts initially in the middle of the left slab. At the fourth step, it hits the wall and is on its way to bouncing back when the boundary between the two slabs disappears. It goes to the right slab with a diminished velocity. When it hits the wall at the far side of the other slab at the seventh step, its momentum is not high enough to overcome the potential well. It bounces back but is trapped into traveling to the right when a new inner wall develops at the nineteenth step.

The pseudonucleon in Fig. 3(c) starts initially in the inner edge with a large momentum. After hitting the wall, it travels in the negative z direction. It hits the far side wall of the left slab and goes to the positive z direction at the eighth step. The disappearance of the boundary allows it to go from the left slab to the right slab at the twelfth step. At the twentieth step, it reaches the new wall formed by the pseudonucleons which spilled over the potential well at the far side of the right slab. Thereafter, it travels from the right slab towards the left slab but is trapped in the right slab by the new wall formed when the two slabs separate.

The pseudoparticle in Fig. 3(d) is initially at the far edge of the left slab and has the smallest momentum. It goes from the left slab to the right slab at the seventh step. Because its energy is not sufficiently high, it is bounced from the far side of the left slab at the thirteenth step and proceeds to move to the left slab. However, it is trapped in the right slab as a new wall is formed in the boundary region at the nineteenth step.

The pseudoparticle in Fig. 3(e) is initially at the center of the left slab. Its small momentum allows it to move only a short distance when a high density region is formed in the region of $z \sim 0$ at the tenth step. The high-density region gives rise to a repulsive local potential which sends the pseudonucleon backward to the negative z direction. When the system separates at the nineteenth step, this pseudonucleon stays in the left slab.

The pseduonucleon in Fig. 3(f) is initially at the inner edge and moves with a small momentum. It is moving to the negative z direction when the boundary disappears. When the inner walls between the slabs are formed at the nineteenth step, they are still in the left slab and remain there.

They dynamics of the pseudoparticles has many interesting features. First, the flow-through motion is indeed initiated by the leading pseudonucleons which overcome the potential and spill over the far side of the other slab.

Second, the trajectories of the fast particles are such that they go from one slab and emerge in the other slab, whereas the slow pseudonucleons are often trapped in their original slab. In other words, the fast pseudonucleons are mainly the ones which are exchanged, while the slow ones are not. This conclusion is consistent with the evolution of the single-particle wave functions as depicted in Fig. 19 of Ref. 6. Such an exchange is the mechanism of the dissipation of the relative momentum of collective translation. For the left slab to exchange a fast pseudonucleon with a momentum $\vec{p}_z$ pointing in the positive z direction in return for a pseudonucleon with a $\vec{p}_z$ pointing in the opposite direction, there is a loss of momentum of $2\vec{p}_z$. Hence, the resultant separating system moves with a much

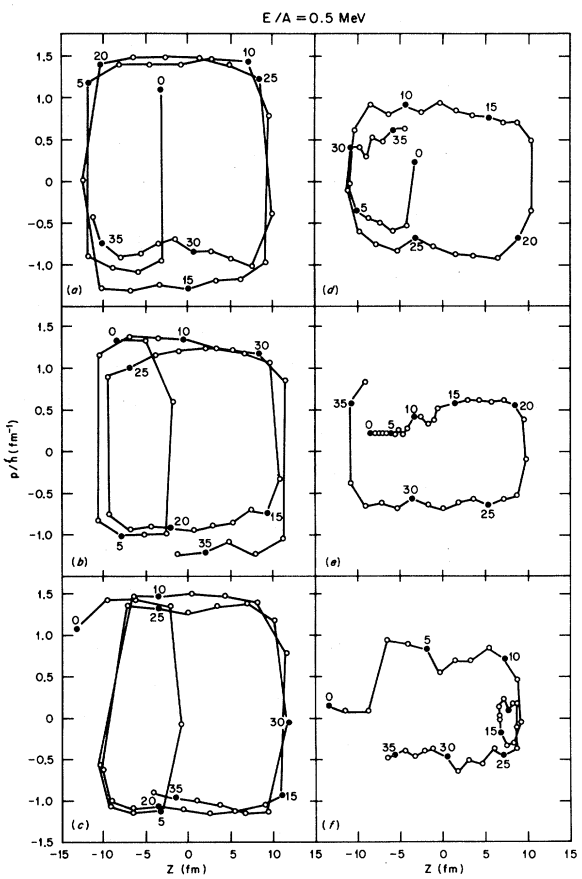

FIG. 4. Same as in Fig. 3 except that the center-of-mass bombarding energy is $E/A = 0.5$ MeV and the time step Δt is 0.0417×10^{-21} sec.

slower speed compared to the initial speed.

The trajectories of some typical pseudonucleons in the left slab for the $E/A=0.5$ MeV collisions are shown in Fig. 4. Here, the time step in the time sequences is $\Delta t=0.0147\times10^{-21}$ sec. The dynamics of the pseudonucleons are quite different from those of the 3.5 MeV case. One observes that even though the fastest pseudonucleons are not much slowed down after traversing from one slab to the other, they do not have enough energy to emerge outside of the potential well at the far side of the other slab. As a result, they are trapped by the outer wall of the slab and follow a confined motion.

IV. THE LOW-l FUSION WINDOW IN TDHF CALCULATIONS

The possibility that nearly-head-on nuclear collisions above the Coulomb barrier may not lead to fusion has been speculated for some time, both from the hydrodynamical viewpoint[40] and the dynamics obtained from TDHF calculations.[6–12] Although the outcome of an absence of fusion is the same, the physical processes involved in this so-called "low-l fusion window" or simply "l window" in the hydrodynamical description and in the TDHF descriptions are different. In the hydrodynamical picture, the low-l fusion window arises when the composite system returns from an extremely pancake shape back to an extremely prolate shape. The predominant source of instability is the Rayleigh instability governed by the ratio of the major to minor radii of the prolate composite system at the moment of maximum stretching.[40] On the other hand, in a TDHF calculation, there is no prominent occurrence of flow in the transverse direction, and thus no formation of pancake shapes at the moment of maximum impact. The occurrence of the breakup appears to follow a flow-through motion in which nuclear matter from one nucleus flows past the nuclear matter of the other nucleus and emerges at the far surface of the other nucleus.[6–13,34] The occurrence of the l window is governed by very different considerations such as the Fermi motion of the nucleons and the depth of the mean-field potential as we shall soon see.

From the TDHF results, we know that the l window occurs at a threshold energy of $E_{\rm lab}=54$ MeV for the $^{16}O+^{16}O$ system and that the l window can be specified by[8,9] an absence of fusion when

$$l\leq\left[\frac{2\mu R_B^{\,2}}{\hbar^2}\left[\frac{E_{\rm lab}-E_{\rm th}}{2}\right]\right]^{1/2}, \tag{4.1}$$

where μ is the reduced mass, R_B is the interaction barrier radius, and $E_{\rm th}$ is the threshold energy in the laboratory system. For the $^{40}Ca+^{40}Ca$ systems, no l window has been observed up to an energy of $E_{\rm lab}=200$ MeV,[9] although other and later calculations indicate a threshold energy at $E_{\rm lab}=195$ MeV.[7] Other TDHF calculations for the low-l fusion window in the $^{28}Si+^{28}Si$ and $^{16}O+^{40}Ca$ systems have also been performed recently.[41] It would be desirable to put this information concerning the l window in the TDHF calculations in a coherent picture, making use of the concepts of pseudoparticle dynamics uncovered in the last section.

Before we proceed to discuss the l window in the case of colliding nuclei, it is worth reviewing the dynamics of the pseudonucleons in a single self-bound fermion system and in colliding nuclei. Understanding the salient features of the pseudonucleon dynamics then allows one to comprehend the physics involved in the occurrence of the l window.

The dynamical motion of the pseudonucleons inside a nucleus is well known and can be easily summarized. The pseudonucleons are distributed in an approximately uniform way in the phase space within the domain $\epsilon_f\leq p^2/2m+\mathcal{V}(\rho(r))$. Each of these pseduonucleons traverses in nearly straight line trajectories in the interior of the nucleus and suffers an elastic reflection at the surface. If the initial spatial and momentum radii are properly chosen (e.g., approximately the same as those obtained in the Hartree-Fock calculation), the subsequent dynamics of these pseudonucleons will lead to the same distribution function and leaves the distribution function time independent. The motion is such that for every group of pseudonucleons leaving a phase space cell, it is replenished by another group from some other location. In the early stages of the collision of two nuclei, the dynamics of the collision are sufficiently complicated that we limit our attention to the pseudonucleons at selected spatial points along the symmetry axis in conjunction with the whole momentum space points. In the configuration space we choose the points A, B, C, D, E, and F (Fig. 5) which are fixed in space. The velocity of the left nucleus is represented by $\vec{v}$, while the velocity of the right nucleus by $-\vec{v}$. The initial distribution function $f(\vec{r}\vec{p})$ at points A, B, C, ..., F in the momentum space are shown in Fig. 5(a). They are Fermi spheres with uniform density shifted by $m\vec{v}$ and $-m\vec{v}$ for the left and the right nucleus, respectively.

There are two effects on the dynamics when the common boundary disappears. First, those pseu-

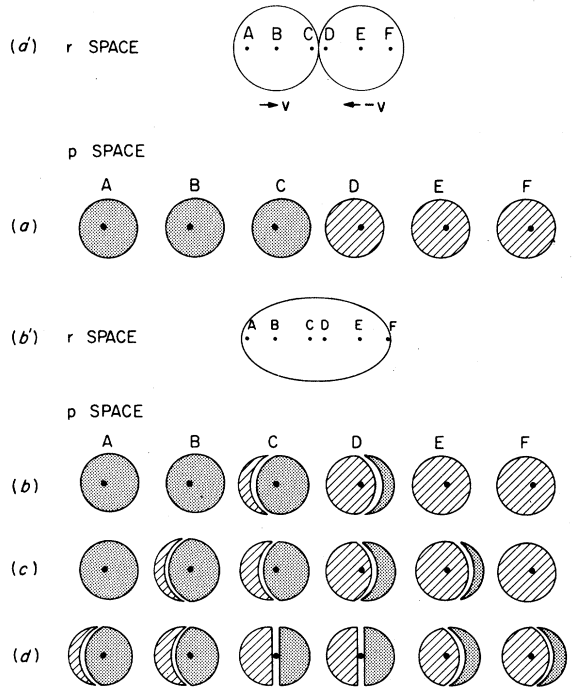

FIG. 5. Spatial and momentum distribution of pseudonucleons in a head-on collision of two equal nuclei. (a') Distribution of spatial density before contact. Points A, B, C, D, E, and F are points fixed in space which we wish to examine. (a) The initial momentum distributions at the sampling points. For points A, B, and C they are Fermi spheres displaced to the right. For points D, E, and F, they are Fermi spheres displaced to the left. (b') The distribution of spatial density at a time when the boundary between the two nuclei disappears. (b) The momentum distribution at the sampling points shortly after the disappearance of the boundary. Pseudonucleons originally from the left nucleus are represented by the dotted region, while pseudonucleons originally from the right nucleus are represented by the shaded region. (c) The momentum distribution at the sampling points at a time $\sim R_0/v_f$ after the boundary between the two nuclei disappears. (d) The momentum distribution at the sampling points at a time $\sim 2R_0/v_f$ after the boundary between the two nuclei disappears. The most energetic pseudonucleons of one nucleus now reach the far surface of the other nucleus.

donucleons originating from point C of the left nucleus and coming to the boundary points will follow a straight line trajectory and proceed to the right nucleus. Second, in the absence of the boundary and the subsequent change of the trajectories of these pseudonucleons, the left part of the original Fermi sphere at C is not replenished by pseudonucleons from the left nucleus. In place of these vacated phase space points now arrive the nucleons from the right nucleus, the most energetic ones being the first to arrive. The distribution of pseudonucleons at point C is no longer a Fermi sphere. It consists of a cap of the most energetic pseudonucleons from the right nucleus and a Fermi sphere of the original left pseudonucleons shaved at the left side [Fig. 5(b)].

At an even later time after the removal of the boundary ($t \sim 2r_0/v_f$), the most energetic pseudonucleons from the right nucleus reach the far surface point A of the left nucleus. Similarly, the most energetic pseudonucleons from the left nucleus reach the far surface point F of the right nucleus [Fig. 5(d)]. They are not expected to suffer much loss of energy in arriving at these surface points. They are now ready to give an assault to the "walls" at points A and F. Whether or not the wall can contain these most energetic pseudonucleons depends on the "height" of the wall and the energy of these pseudonucleons. Furthermore, besides these pseudonucleons that have just arrived, a large array of energetic pseudonucleons originally from the other nucleus have positioned themselves at more distant points (e.g., B and C) to prepare for an assault of the wall at a later time. Such a "collective" behavior of the pseudonucleons is a consequence of the initial condition (of colliding nuclei).

The wall of the composite system corresponds to the boundary of the mean-field potential. A very important characteristic of the "wall" is the depth of the potential well. The motion of the most energetic pseudonucleons depends on whether their kinetic energy (measured relative to a wall at rest) is such that they are bound or unbound with respect to the mean-field potential well. If these nucleons are bound inside the potential, they are then reflected backward by the potential after proceeding to the classical turning point and are therefore contained in the nuclear system. The containment of these pseudonucleons will eventually lead to a fused compound system. On the other hand, if the energy is such that they are unbound in the mean-field potential, they will proceed forward and emerge outside of the surface point. When this happens, the pseudonucleons which emerge outside will lower the potential well at the new points because of the self-consistency effect. The turning points of many of the other pseudonucleons are shifted in the direction of the emerging nucleons so that more pseudonucleons emerge out of the far side of the surface. This will lower the potential even more to allow more and more pseudonucleons to emerge outward. It is reasonable to expect from the results of

the last section that such a coherent flow-through motion will continue on and give rise to the nonfusion (breakup) events in the low-l fusion window of the TDHF calculations. Whether such a flow-through motion of pseudonucleons emerging at the far side of the other nucleus is indeed the origin of this low-l fusion window can be inferred by comparing the threshold energies for flow-through motion and the l windows obtained in the TDHF calculations. Good agreement between these quantities will indicate that the coherent flow-through motion is likely the origin of the l window.

We can estimate the threshold energy for the occurrence of the flow-through motion. The momentum of the most energetic pseudonucleons has the magnitude $\hbar k_f + m v_0$ where v_0 is the initial speed of one of the nuclei in the center-of-mass system. The momentum relative to the potential at the far surface points is $\hbar k_f + m(v_0 - v_w)$ where v_w is the velocity of the surface point and is taken to be directing in the same direction as the initial velocity v_0. The flow-through motion occurs when these most energetic pseudonucleons become unbound. That is, when

$$\frac{\hbar^2}{2m}[k_f + m(v_0 - v_w)/\hbar]^2 \geq \frac{\hbar^2}{2m}k_f^2 + B \ , \quad (4.2)$$

where B is the separation energy of the ground-state nucleons. Equation (4.2) leads to

$$\tfrac{1}{2}m(v_0 - v_w)^2 \geq [(1+B/F)^{1/2} - 1]^2 \epsilon_f \ , \quad (4.3)$$

where ϵ_F is the Fermi energy $\hbar^2 k_f^2/2m$. The velocity at the surface point v_w when the most energetic pseudonucleons arrive there is difficult to estimate. However, in the range of about 1 MeV per nucleon which is the range of the threshold energy we are considering for the l window, the nuclear systems are not much compressed. Because of the near incompressibility of the nuclear matter, the outer walls of the colliding nuclei are brought to a near halt in the center-of-mass system soon after contact. The velocities v_w when the most energetic nucleons arrive are expected to be small in the center-of-mass system and can therefore be neglected there. Accordingly, in the center-of-mass system, the threshold kinetic energy per nucleon for the flow-through motion is roughly

$$\tfrac{1}{2}m v_0^2 \gtrsim [(1+B/\epsilon_f)^{1/2} - 1]^2 \epsilon_F \ . \quad (4.4)$$

Upon using a separation energy of $B = 8$ MeV and $\epsilon_F = 35$ MeV, one finds the threshold energy per nucleon in the center-of-mass system given by

$$\tfrac{1}{2}m v_0^2 \gtrsim 0.411 \text{ MeV} \ . \quad (4.5)$$

The foregoing consideration can be generalized to non-head-on collisions in the presence of Coulomb repulsion. As part of the energy is expended in overcoming the Coulomb and centrifugal barriers, the Fermi spheres are displaced in the radial direction by an amount $m v_r$ given by

$$\tfrac{1}{2}\mu(2v_r)^2 = E_{\text{c.m.}} - \frac{\hbar^2 l^2}{2\mu R_B^2} - \frac{Z_1 Z_2 e^2}{R_B} \ , \quad (4.6)$$

where μ is the reduced mass of the two nuclei and R_B the separation between the two nuclei at the interaction barrier. All the considerations concerning the emergence of the most energetic pseudonucleons remain the same as in the head-on collision. Thus, flow-through motion of the two will take place when

$$\tfrac{1}{2}m v_r^2 = \left[E_{\text{c.m.}} - \frac{\hbar^2 l^2}{2\mu R_B^2} - \frac{Z_1^2 e^2}{R_B}\right] \Big/ 2A_1 \gtrsim [(1+B/\epsilon_F)^{1/2} - 1]^2 \epsilon_F \ , \quad (4.7)$$

where we have neglected the velocity of the surface points. Thus, for the case of a collision of two equal nuclei each with mass number A_1 and atomic number Z_1, flow-through motion takes place when the energy exceeds the threshold value

$$E_{\text{c.m}}(\text{threshold}) \cong \frac{Z_1^2 e^2}{R_B} + [(1+B/\epsilon_f)^{1/2} - 1]^2 \epsilon_F \times 2A_1 \ . \quad (4.8)$$

When this energy is exceeded, there is an l window for the flow-through motion leading to the breakup of the nuclei when l satisfies

$$l^2 \lesssim \frac{2\mu R_B^2}{\hbar^2}\left\{E_{\text{c.m.}} - \frac{Z_1^2 e^2}{R_b} - [(1+B/\epsilon_f)^{1/2} - 1]^2 2A_1 \epsilon_F\right\} . \quad (4.9)$$

which agrees with the expression Eq. (4.1) obtained for l^2 from TDHF calculations.[8,9]

For unequal nuclei, we focus our attention again on the center-of-mass system. The displacements of the Fermi spheres are now different for the points in either nuclei, being greater for the lighter nuclei. The most energetic pseudonucleons in the lighter nucleus have energies different from the most energetic pseudonucleons in the heavier nucleus. Again, the emergence of pseudonucleons at the far surfaces of *both* nuclei will occur and lead to the flow-through motion when the energies of these most energetic pseudonucleons of *both* nuclei are such that they become unbound. Using arguments similar to those given previously, one finds that flow-through motion occurs when

$$\left[E_{\text{c.m.}}-\frac{\hbar^2 l^2}{2\mu {R_B}^2}-\frac{Z_1 Z_2 e^2}{R_B}\right]\Big/\left[\frac{A_2(A_1+A_2)}{A_1}\right]\gtrsim\left[\left[1+\frac{B}{\epsilon_f}\right]^{1/2}-1\right]^2\epsilon_F\ , \tag{4.10}$$

where $A_2 \geq A_1$. This inequality leads to the threshold energy as given by

$$E_{\text{c.m.}}(\text{threshold})\cong\frac{Z_1 Z_2 e^2}{R_B}+\frac{A_2(A_1+A_2)}{A_1}[(1+B/\epsilon_F)^{1/2}-1]^2\epsilon_F \tag{4.11}$$

and the l window below which no fusion occurs as

$$l^2\lesssim\frac{2\mu {R_B}^2}{\hbar^2}\left\{E_{\text{c.m.}}-\frac{Z_1 Z_2 e^2}{R_B}-\frac{A_2(A_1+A_2)}{A_1}[(1+B/\epsilon_F)^{1/2}-1]^2\epsilon_F\right\}. \tag{4.12}$$

How good are the above estimates of the threshold energies compared with the results from the TDHF calculations? Clearly, the estimates we presented are obtained in a much simplified picture of the dynamics; thus, only a qualitative agreement is expected. This is especially so in view of the neglect of the surface velocity at the moment when the most energetic pseudonucleons make an assault on the surface. We can examine the $^{16}O+{}^{16}O$ system. Using $B=8$ MeV, $\epsilon_F=35$ MeV, and a radius parameter $r_0=1.2$ fm, we find

$$E_{\text{c.m.}}(\text{threshold})=28.40\ \text{MeV}\ , \tag{4.13}$$

which is close to what is obtained in the TDHF calculation (Table I). Furthermore, the relation between $E_{\text{c.m.}}$ and l, as given by Eq. (4.9), is the same as what was given previously by Eq. (4.1).

For $^{28}Si + {}^{28}Si$, $^{16}O + {}^{40}Ca$, and also $^{40}Ca + {}^{40}Ca$, we use the same binding energy B and ϵ_F and obtain the threshold energies as given in Table I. They compare favorably with those obtained from the TDHF calculations. For the $^{12}C + {}^{12}C$ system, a different interaction was used[10] and the important parameters of B and ϵ_f which are interaction dependent and enter into the estimates of the threshold energies should rather be $B\sim 12$ MeV and

TABLE I. Threshold energies for the onset of no fusion in head-on collisions.

Systems	Threshold energy $E_{\text{c.m.}}$ in MeV from our model [Eqs. (4.8) and (4.11)]	Threshold energy $E_{\text{c.m}}$ in MeV from TDHF
$^{16}O + {}^{16}O$	28.40	27[a]
$^{28}Si + {}^{28}Si$	61.76	55[b]
$^{16}O + {}^{40}Ca$	89.86	100[b]
$^{40}Ca + {}^{40}Ca$	103.08	97.5[c]
$^{12}C + {}^{12}C$	36.5[d]	35.0[e]

[a]Reference 9.
[b]Reference 41.
[c]Reference 7.
[d]We use a different set of B and ϵ_f as different interactions are used in Ref. 10.
[e]Reference 10.

$\epsilon_f \sim 23$ MeV.[42] When this set of parameters is used in Eq. (4.8), one obtains the threshold energy which agrees well with the results from TDHF calculations.[10] Such agreement between the threshold energies for the onset of flow-through motion and the TDHF results for the onset of no fusion events indicates the approximate validity of the simple picture that the emergence of the most energetic nucleons of one nucleus at the far surface of the other nucleus initiates a coherent flow-through motion leading to the breakup of the composite system.

It is worth pointing out that the picture that a flow-through motion leads to the breakup of the composite system is good *only* for the "first chance" breakup events which are presumably what have been reported in the TDHF calculations discussed in this section. It is known that some colliding systems which appear to be separated after the collision subsequently recombine again when the TDHF dynamics are allowed to proceed further (see Fig. 10 of Ref. 6). The occurrence of a recombination is a result of having the phases of different types of motion properly matched. Therefore, a recombination after a flow-through motion is expected to be rather localized in energy and angular momentum space. An investigation of these recombinations and the subsequent ("second chance") breakup events clearly requires a relation concerning the flow-through motion and the final fusion or breakup of the composite system different from what is presented here.

With regard to the experimental search of the low-l fusion window, there is the observation of two components of fragments in the deep-inelastic scattering of $^{32}S + {}^{27}Al$ which differ by 20 MeV in Q value. This observation gave possible indirect evidence for the existence of the low-l fusion window,[43] although another explanation of the phenomena is also possible. There is also another experimental observation in the energy loss in the collision of ^{16}O on ^{16}O which suggests the presence of the l window.[44] On the other hand, preliminary results on the direct-measurement of the total fusion cross secton of $^{16}O + {}^{40}Ca$ appear to give no indication of the onset of the l window.[45]

It is of interest to note that the low-l fusion window can be well utilized to provide an experimental test on the validity of the TDHF approximation. The threshold energy and the l dependence are now understood as depending on the emergence of the most energetic nucleons from the far surface. In the mean-field collisionless approximation, the most energetic nucleons suffer little energy loss in reaching the far surface. It is thus easy to understand that if the collision of nucleons is allowed, as, for example formulated in the extended TDHF approximation,[4] there is a finite probability for the most energetic nucleons to suffer a loss of radial kinetic energy before reaching the far surface because of particle collisions. The loss of radial kinetic energy may be sufficient to cause this group of nucleons to be trapped inside the potential wall when the wall is attacked. In such a case, what in the collisionless TDHF case will lead to the flow-through motion and the subsequent breakup may become a case of fusion in the presence of particle collisions. One expects therefore that with the inclusion of the particle collisions, the onset of the occurrence of no fusion in a head-on collision will move to a higher energy. A careful search for the l window for various systems and a subsequent comparison with the results from TDHF calculations will indicate either the validity of the TDHF approximation or the need to introduce particle collisions.

It is worth noting that although the procedures used in estimating the threshold energy for the occurrence of the l window bear some resemblance to those used in estimating the onset of the "Fermi jet,"[21] there are important differences. In our consideration of the l window, we assume that the wall speeds are negligible in the *center-of-mass system* and that the self-consistency leads to the flow-through motion when the potential well is surpassed. These assumptions are different from those in the usual consideration of the "Fermi jet."[21]

In the case of two unequal nuclei, the most energetic leading pseudonucleons from the lighter nucleus has a greater energy than the most energetic leading pseudonucleon from the heavier nucleus because of the difference in the speeds of the two nuclei in the center-of-mass system. The results (4.10)–(4.12) are obtained for the flow-through motion when the most energetic pseudonucleons from *both* nuclei become unbound. What happens when only the most energetic leading nucleons of one of the nuclei (the lighter nucleus) become unbound? This happens when

$$\frac{A_1(A_1+A_2)}{A_2}E_0 \le E_{\text{c.m.}} - \frac{\hbar^2 l^2}{2\mu R_B{}^2} - \frac{Z_1 Z_2 e^2}{R_B} \le \frac{A_2(A_1+A_2)}{A_1}E_0 , \tag{4.14}$$

where $A_2 \ge A_1$, and

$$E_0 = [(1+B/\epsilon_F)^{1/2}-1]^2\epsilon_f .$$

It is reasonable to expect that as the most energetic leading pseudonucleon from the heavier nucleus cannot escape the potential at the far side of the light nucleus, a fused system will result. However, because the energetic pseudonucleons from the light nucleus become unbound when they reach the far side of the heavier nucleus, there is a substantial emission at the far side of the heavier nucleus. Based on such a picture, particle emission accompanying fusion is expected (1) to occur in the energy range given by Eq. (4.14), (2) to be found in the direction of motion of the lighter nucleus but not in the direction of motion of the heavier nucleus, and (3) to be absent in the collision of two equal nuclei where the occurrence of particle emission is immediately followed by the flow-through motion. Recent theoretical[46] and experimental[47] results do indicate the occurrence of preequilibrium particle emission accompanying fusion reactions. It will be of interest to examine whether the systematics obtained there follow Eq. (4.14) given above.

There is, however, another explanation given for the low-l fusion window in the TDHF calculations in terms of the tensile strength of nuclear matter.[48] It is argued that the breakup occurs when the tensile strength of nuclear matter is exceeded. Such an explanation focuses its attention at the late stages of the dynamics before breakup, while the explanation we have given focuses its attention at the initial stage of the flow-through motion. So far, the latter consideration appears to be sufficient to allow an estimate of the low-l fusion threshold in light systems. Whether the tensile strength consideration needs to enter in heavy systems remains to be seen.

V. SUMMARY AND CONCLUSIONS

We undertake a study of the time-dependent Hartree-Fock approximation from a classical viewpoint in order to facilitate comparison of the time-dependent Hartree-Fock approximation with other classical theories and to help guide our intuition in understanding the underlying physics. The path we take in going from the TDHF approximation to a classical description is a very well-known one. Instead of using either the density matrix or the single-particle wave functions, we employ the Wigner function which is analogous with, but not identical to, the classical distribution function of spatial and momentum coordinates. Upon making the approximate interpretation of the Wigner function as indeed the classical distribution and expand the equation of motion to the lowest-order term of inhomogeneity in the force field, we obtain the main result that the time-dependent Hartree-Fock approximation is approximately equivalent to a purely classical pseudoparticle simulation. In this simulation, a collection of pseudoparticles is introduced to discretize the phase space. The dynamics are completely determined by following the pseudoparticle trajectories which turn out to be exactly the same as the classical collisionless trajectories of real particles moving in the self-consistent field.

We next apply the pseudoparticle simulation to a concrete one-dimensional numerical example to bring out the salient features of the pseudoparticle dynamics. Pseudoparticle trajectories are traced to see their motion in a fusion and a breakup reaction.

The dynamical motion of the pseudonucleons inside a nucleus can be easily inferred. The pseudonucleons are distributed in an approximately uniform way in the phase space within a finite domain, the uniformity being a consequence of the Pauli exclusion principle. Each pseudonucleon traverses in nearly straight-line collisionless trajectories in the interior of the nucleus and suffers an elastic reflection at the surface. Such a description of the dynamics of nucleons is not new. It is embodied in the discussion of the Fermi motion of nucleons and also in the theory of one-body dissipation.[21,34] What is perhaps new is to see how such a motion can be inferred from the TDHF approximation and thereby connected to a dynamical theory.

An important concept in the description of a ground-state nucleus is the replenishment of the Fermi spheres under the motion of the pseudonucleons. The total distribution function of a ground-state nucleus is time independent. Such time independence is achieved in the presence of the motion of pseudonucleons when the motion is such that for every group of pseudonucleons leaving a phase space point, it is replenished by the arrival of another group of pseudonucleons from some other location. Thus, a change of the trajectories of the pseudonucleons will affect the replenishment of the Fermi sphere.

We next focus our attention to the TDHF results of absence of fusion in head-on collisions when the energy exceeds a certain limit. The disappearance of the boundary between the two nuclei alters the trajectories of the pseudonucleons. The pseudonucleons at the surface with the correct momentum direction can proceed to the other nucleus. They do not replenish the Fermi sphere in its own nucleus but rather add on to the momentum distribution at

another point in the other nucleus. The important instant which determines fusion or nonfusion events occurs when the most energetic pseudonucleons arrive at the far surface of the other nucleus. If these pseudonucleons are contained by the potential well, they will be reflected backward and eventually lead to a fused composite system. On the other hand, if they are not contained but emerge outside the surface, a self-consistent effect develops to lower the potential well to allow even more pseudonucleons to emerge outside the surface. This flow-through motion leads eventually to the breakup of the composite system. Threshold energies and low-l fusion windows obtained using such a picture give good agreement with the TDHF results. Threshold energies for particle emission are also estimated.

Our comparison of the pseudoparticle model with the theory of one-body dissipation reveals the similarities and differences. The similarities can be found in the description of the trajectories, while the differences are in the additional assumptions of the one-body dissipation with regard to energy dissipation. Furthermore, the pseudoparticle simulation is a complete and self-contained microscopic dynamical theory all by itself without the need to attach itself to some other dynamical theory of collective variables, as is the case with the theory of one-body dissipation.

The pseudoparticle simulation can also be compared with the classical particle model used in the discussion of high-energy, heavy-ion collisions. The similarity of the two descriptions can be found in the way the trajectories of the particles are followed. However, in the pseudoparticle model, the particles are pseudoparticles, so they can be numerous in number, whereas in the classical particle model, the particles are real particles, the same number as the mass number of the nucleus. Another difference can be found in the treatment of the Pauli principle. In the pseudoparticle model, this is done by giving an initial Fermi distribution in the momentum space, while in the other treatment, a momentum-dependent potential is used to simulate the Pauli exclusion effect.[30] Still another difference is the possibility of incorporating the equation of state using the mean-field potential in the pseudoparticle simulation.

Useful as it is in providing a conceptual tool in understanding the TDHF approximation, the pseudoparticle simulation may be limited in its practical application because of the large number of pseudoparticles needed to describe the phase-space distribution and the possibility of numerical instability associated with the Vlasov equation. Much work remains to be done to examine whether it can be a useful numerical tool for heavy-ion collisions.

It will be of interest in future work to extend the pseudoparticle simulation to include particle collisions in a way similar to what was done in the Landau-Fermi liquid theory. Such an extension will allow one to discuss the approach to local thermal equilibrium and the validity of hydrodynamical approximations in heavy-ion collisions.

After the main work was completed and the main results were presented[5] the author was happy to learn of recent applications of the pseudoparticle method by G. Maddison and D. Brink.[49] A different approach to study the Vlasov equation was recently developed by H. Tang *et al.*[50]

The author wishes to thank Dr. K. T. R. Davies, Dr. G. R. Satchler, Dr. M. W. Guidry, Dr. K. T. Tsang, Dr. T. A. Welton, Dr. S. Köhler, Dr. S. E. Koonin, and Dr. R. Y. Cusson for stimulating and helpful discussions.

[1]C. Y. Wong, J. A. Maruhn, and T. A. Welton, Nucl. Phys. A253, 469 (1975).

[2]C. Y. Wong, T. A. Welton, and J. A. Maruhn, Phys. Rev. C 15, 1558 (1977); C. Y. Wong, *ibid.* 17, 1832 (1978).

[3]C. Y. Wong and J. A. McDonald, Phys. Rev. C 16, 1196 (1977).

[4]C. Y. Wong and H. H. K. Tang, Phys. Rev. Lett. 40, 1070 (1978); Phys. Rev. C 20, 1419 (1979).

[5]The main results of the present article were presented previously in C. Y. Wong, *Time-Dependent Hartree-Fock Method,* edited by P. Bonche, B. Giraud, and Ph. Quentin (Editions de Physique, Paris, 1979), p. 205.

[6]P. Bonche, S. E. Koonin, and J. W. Negele, Phys. Rev. C 3, 1226 (1976).

[7]S. E. Koonin, K. T. R. Davies, V. Maruhn-Rezwani, H. Feldmeier, S. J. Krieger, and J. W. Negele, Phys. Rev. C 15, 1359 (1977).

[8]H. Flocard, S. E. Koonin, and M. S. Weiss, Phys. Rev. C 17, 1682 (1978).

[9]P. Bonche, B. Grammaticos, and S. Koonin, Phys. Rev. C 17, 1700 (1978).

[10]R. Y. Cusson, R. K. Smith, and J. A. Maruhn, Phys. Rev. Lett. 36, 1166 (1976); R. Y. Cusson and J. A. Maruhn, Phys. Lett. 62B, 134 (1976); R. Y. Cusson and J. A. Maruhn, *ibid.* 62B, 134 (1976); J. A. Maruhn

and R. Y. Cusson, Nucl. Phys. A270, 437 (1976).
[11]J. W. Negele, S. E. Koonin, P. Møller, J. R. Nix, and A. J. Sierk, Phys. Rev. C 3, 1098 (1978).
[12]J. W. Negele, in *Theoretical Methods in Medium-Energy and Heavy-Ion Physics,* edited by K. W. McVoy and W. A. Friedman (Plenum, New York, 1978), p. 235.
[13]Recent work in TDHF is discussed in *Time-Dependent Hartree-Fock Method,* edited by P. Bonche, B. Giraud, and Ph. Quentin (Editions de Physique, Paris, 1979).
[14]P. C. Lichtner and J. J. Griffin, Phys. Rev. Lett. 37, 1521 (1976); P. C. Lichtner, J. J. Griffin, H. Schulteis, R. Schulteis, and A. B. Volkov, University of Maryland Report ORO-5126-49, 1978; J. J. Griffin, University of Maryland Report ORO-5126-44, 1978.
[15]J. Blocki and H. Flocard, Nucl. Phys. A273, 45 (1976).
[16]K. K. Kan, J. J. Griffin, P. C. Lichtner, and M. Dworzecka, in *Time-Dependent Hartree-Fock Method,* edited by P. Bonche, B. Giraud, and Ph. Quentin (Editions de Physique, Paris, 1979).
[17]C. M. Shakin and M. S. Weiss, UCRL Report No. 08500.
[18]H. Orland and R. Schaeffer, Z. Phys. A 290, 191 (1979).
[19]S. Levit, J. W. Negele, and Z. Paltiel, Phys. Rev. C 21, 1603 (1980); 22, 1979 (1980).
[20]Y. Alhassid and S. E. Koonin, Phys. Rev. C 23, 1590 (1981).
[21]J. Błocki, Y. Boneh, J. R. Nix, J. Randrup, M. Robel, A. J. Sierk, and W. J. Swiatecki, Ann. Phys. (N. Y.) 113, 330 (1978).
[22]S. E. Koonin, R. L. Hatch, and J. Randrup, Nucl. Phys. A283, 87 (1977); S. E. Koonin and J. Randrup, *ibid.* A289, 475 (1977).
[23]L. Wilets, A. D. MacKellar, and G. A. Rinker, Proceeding of the Symposium on Macroscopic Features of Heavy-Ion Collisions, Argonne, Illinois, 1976, ANL Report No. ANL-PHY-76-2.
[24]A. R. Bodmer and C. N. Panos, in Proceedings of the International Workshop III on Gross Properties of Nuclei and Nuclear Excitations, Hirschegg, Kleinwalsertal, Austria, 1975, edited by W. D. Meyers, Technische Hochschule Darmstadt Report No. AED-Conf. 75-009-000, 1975 (unpublished); Phys. Rev. C 15, 1342 (1977).
[25]J. P. Bondorf, H. T. Feldmeier, S. Garpman, and E. C. Halbert, Phys. Lett. 65B, 217 (1976); J. P. Bondorf, P. J. Siemens, S. Garpman, and E. C. Halbert, Z. Phys. A 279, 385 (1976).
[26]R. K. Smith and M. Danos (unpublished).
[27]Y. Yariv and Z. Fraenkel, Phys. Rev. C 20, 2270 (1979).
[28]J. Cugnon, T. Mitzutani, and J. Vandermeulen, Nucl. Phys. A352, 505 (1981).
[29]J. Cugnon, Phys. Rev. C. 22, 1885 (1980); 23, 2094 (1981).
[30]L. Wilets, E. M. Henley, M. Kraft, and A. D. MacKellar, Nucl. Phys. A282, 341 (1977).
[31]L. Wilets, Y. Yariv, and R. Chestnut, Nucl. Phys. A301, 359 (1978).
[32]E. Wigner, Phys. Rev. 40, 749 (1932).
[33]E. A. Remler, Ann. Phys. (N. Y.) 95, 455 (1975); E. J. Heller, J. Chem. Phys. 65, 1289 (1976).
[34]G. F. Bertsch, Nucl. Phys. A249, 253 (1975); Lecture Notes for the 1977 Les Houches Summer School, Les Houches, France.
[35]S. E. Koonin, Ph.D thesis, MIT, 1975 (unpublished).
[36]J. P. Hansen and I. R. McDonald, *Theory of Simple Liquids* (Academic, New York, 1976), Chap. 3 and references cited therein.
[37]H. Okuda, Nucl. Sci. Eng. 64, 1 (1977) and references cited therein; C. Z. Cheng and H. Okuda, Nucl. Fusion 18, 5 (1978); W. W. Lee and H. Okuda, J. Comp. Phys. 26, 2 (1978).
[38]N. L. Balazs and G. C. Zipfel, J. Math. Phys. 15, 2086 (1974); N. L. Balazs and H. C. Pauli, Z. Phys. A 281, 395 (1977).
[39]S. Köhler and H. Flocard, Nucl. Phys. A323, 189 (1979).
[40]J. J. Griffin and C. Y. Wong, Proceedings of the XIV International Winter Meeting on Nuclear Physics, Bormio, Italy, 1976; also University of Maryland Report 76-118.
[41]P. Bonche, K. T. R. Davies, B. Flanders, H. Flocard, B. Grammaticos, S. E. Koonin, S. J. Krieger, and M. S. Weiss, Phys. Rev. C 20, 641 (1979).
[42]R. Y. Cusson, private communication.
[43]J. B. Natowitz, G. Donkellis, B. Kolb, G. Rosner, and Th. Walcher, Heidelberg report (unpublished).
[44]A. Lazzarini, *et al.,* Workshop on Nuclear Dynamics, Granlibakken, California, 1980, Lawrence Berkely Laboratory Report LBL-10688, p. 61.
[45]F. Plasil, private communication.
[46]K. R. Sandhya Devi, M. R. Strayer, K. T. R. Davies, S. E. Koonin, and A. K. Dhar, Phys. Rev. C 24, 2521 (1981).
[47]D. G. Sarantites, L. Westerberg, M. L. Halbert, R. A. Dayras, D. C. Hensley, and J. H. Barker, Phys. Rev. C 18, 778 (1978); K. Geoffroy Young, D. G. Sarantites, J. R. Beene, M. L. Halbert, D. C. Hensley, R. A. Dayras, and J. H. Barker (unpublished); G. A. Pettit, R. L. Ferguson, A. Gavron, F. E. Obenshain, F. Plasil, A. H. Snell, G. R. Young, K. A. Geoffroy D. G. Sarantites, and C. F. Maguire, Proceedings of International Symposium on Continuum Spectra of Heavy-Ion Reactions, San Antonio, Texas, 1979 (unpublished).
[48]G. F. Bertsch, Phys. Rev. C 17, 1646 (1978).
[49]G. Maddison and D. Brink (unpublished).
[50]H. Tang, C. H. Dasso, H. Ebensen, R. A. Broglia, and A. Winther, Phys. Lett. 101B, 10 (1981).